ECS Transactions, 45 (7) 221-229 (2012)
10.1149/1.3701542 ©The Electrochemical Society

Structural and optoelectronic properties of GZO/SiO_x bilayer films by atmosphere pressure plasma jet

Kow-Ming Chang[a,b], Po-Ching Ho[a], Chi-Wei Wu[a], Chin-Jyi Wu[c], Chia-Chiang Chang[c]

[a] Department of Electronics Engineering & Institute of Electronics, National Chiao Tung University, 1001 Ta Hsueh Road, Hsinchu, Taiwan 30010, R.O.C.
[b] College of Electrical and Information Engineering, I-Shou University, No.1, Sec. 1, Syuecheng Rd., Dashu Township, Kaohsiung County, Taiwan 84001, R.O.C.
[c] Industrial Technology Research Institute, Mechanical and Systems Research Laboratories, Hsinchu, Taiwan 310, R.O.C.

Using simple technique to obtain high haze and high conductivity TCO films to enhance optical absorption for silicon thin film solar cell is important. The bilayer GZO film of high haze and low resistivity is achieved by atmosphere pressure plasma jet (APPJ). Thickness of bilayer GZO film was thinner than Asahi-U type FTO film and this result indicated that the APPJ deposition technique has lower material comsumption. The minimum resistivity of 6.00×10^{-4} was achieved at 8 at% gallium doping. X-ray diffraction spectrum showed that an increase in scanning times led to an increase in crystallinity of bilayer GZO films. The bilayer GZO film has much higher haze value in the visible and NIR regions as compared to Asahi U-type FTO film.

Introduction

Transparent conductive oxide (TCO) has attracted substantial attention due to its widely applications, such as solar cells (1-3), flat-panel displays and light emitting diodes. Inside the silicon thin film solar cell, amorphous silicon (a-Si) and microcrystalline silicon (μc-Si) thin films are two important absorber materials. Owing to reducing light-induced degradation, the a-Si thin film should be deposited as thin as possible. The μc-Si thin film is indirect and has low absorption coefficient, so the thickness of it should be deposited thick enough to completely absorb sunlight during single path. In order to fulfil above requirements, it is necessary for development of high haze and high conductivity of the TCO coatings to enhance optical absorption in terms of light trapping (4-7). Using simple technique to obtain high haze and high conductivity TCO films is important. However, the manufacturing processes of commercial Asahi U-type (SnO_2:F) TCO glass demand high deposition temperature and use expensive toxic gas. This study develops the TCO films by the atmosphere pressure plasma jet (APPJ). Several advantages of the APPJ deposition system include low cost, low temperature processes and application in large area applications (8). The influence of physical properties of SiO_x on the growth of GZO films was investigated.

Experimental

In this study, silicon suboxide (SiO_x) was used as buffer layer to increase light scattering ability of GZO films. After the SiO_x buffer layer was deposited on glass, the following GZO layer was deposited on it. Both SiO_x and GZO films were deposited and

Downloaded on 2014-04-28 to IP 140.113.38.11 address. Redistribution subject to ECS terms of use (see ecsdl.org/site/terms_use) unless CC License in place (see abstract).

scanned over an area of 36 cm^2 by APPJ. Figure 1 shows schematic diagram of the experimental equipments for SiO_x and GZO. Hexamethyl-disiloxane (HMDSO) was used as monomer and argon gas as carrier gas to deposit SiO_x films. In order to investigate the influence of carrier gas flow rate on SiO_x buffer layers, flow rates of argon carrier gas were varied as 0, 30 and 60 sccm. The flow rate of CDA main gas was fixed at 40 SLM. The plasma power was set at 450W and substrate temperature was kept at 75°C. GZO films were deposited on SiO_x-coated glasses using zinc acetate and gallium nitrate as precursors for Zn and Ga ions, respectively. The precursor solution was ultrasonically atomized at 2.45 MHz into mist and then carried by nitrogen gas through plasma discharging area connected to a DC pulse power supply. The plasma power was set at 625W and substrate temperature was fixed at 150°C. The flow rates of N_2 carrier gas and main gas were fixed at 300 sccm and 35 SLM, individually. Scanning number of APPJ was varied as 10, 15 and 20 times owing to obtaining optimal GZO film.

Surface morphologies and thicknesses of SiO_x buffer layers and GZO films were analyzed by scanning electron microscope (SEM). The roughness was determined by a DI Digital DI-D3000 atomic force microscopy (AFM). Electrical properties of GZO films were analyzed by Hall measurement. The optical transmittance and haze values were measured by using UV-vis-NIR spectrophotometer. Grazing incidence X-ray diffraction (GIXRD) spectrum of GZO films were measured using x-ray diffractometer.

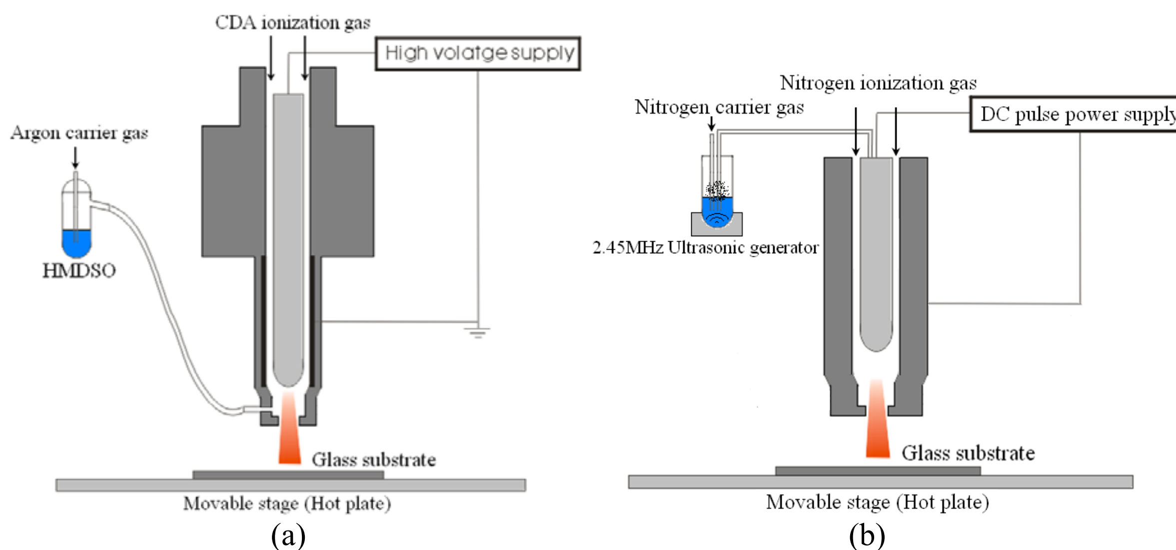

Figure 1. Schematic diagram of the experimental equipment for (a)SiO_x (b)GZO.

Results and Discussion

SiO_x buffer layer effect

Figure 2 shows surface and cross-sectional SEM images of SiO_x buffer layers deposited for different argon carrier gas flow rates, 30 and 60sccm. At flow rates of argon carrier gas, 30 and 60 sccm, thicknesses of SiO_x thin films were 20 and 36 nm, respectively. Root mean square (RMS) roughnesses of the SiO_x buffer layers deposited at argon carrier gas flow rates of 30 and 60 sccm, were 12.20 and 34.87 nm, respectively. Thicknesses and RMS roughness of SiO_x thin films increase as argon carrier gas flow rates increase.

Downloaded on 2014-04-28 to IP 140.113.38.11 address. Redistribution subject to ECS terms of use (see ecsdl.org/site/terms_use) unless CC License in place (see abstract).

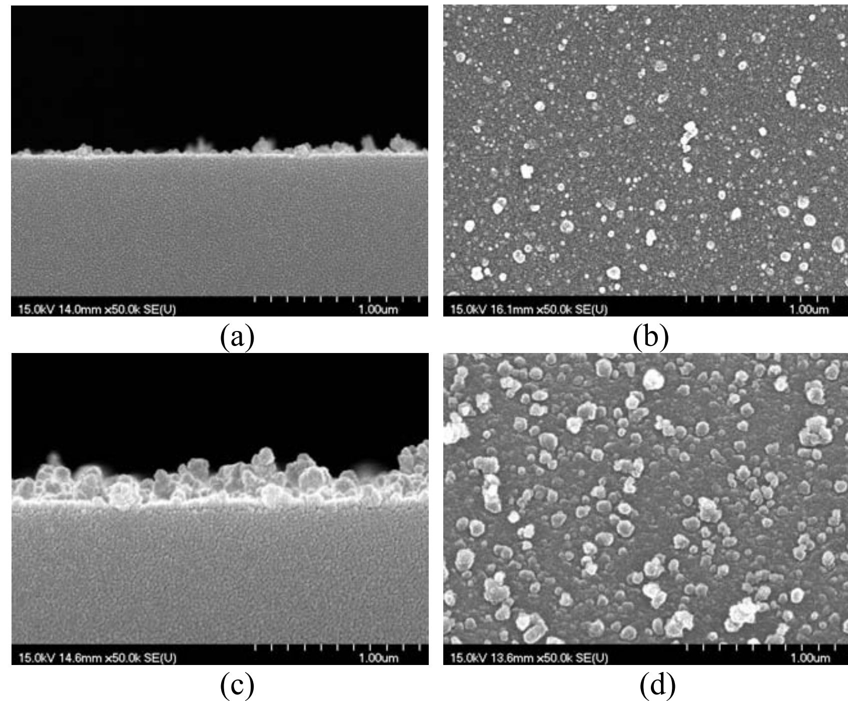

(a) (b)

(c) (d)

Figure 2. Cross-sectional and surface SEM images of SiO_x buffer layers deposited by using different Ar carrier gas flow rate (a,b)30sccm (RMS=12.20nm) (c,d)60sccm (RMS=34.87nm).

Figure 3 dipics transmittance and haze spectra of conventional GZO film and bilayer GZO films using SiO_x as buffer layers, which were deposited at argon carrier gas flow rates of 30 and 60 sccm. With the increase in argon carrier gas flow rates, transmittance of bilayer GZO films decreased because of thicker SiO_x buffer layer, as shown in Fig. 3a. Figure 3b shows haze values of bilayer GZO films in visible region have a significant increase compared with conventional GZO.

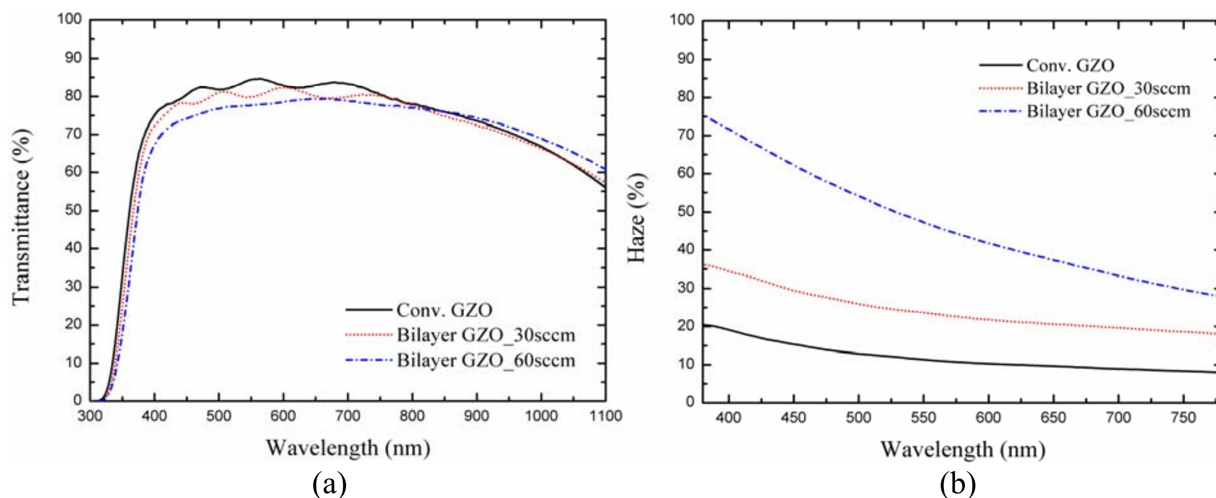

(a) (b)

Figure 3. (a)Transmittance and (b) haze spectra of conventional GZO film and bilayer GZO films deposited on SiO_x buffer layers for different carrier flow rates. Conventional GZO film and bilayer GZO films were scanned 20 times by APPJ.

Downloaded on 2014-04-28 to IP 140.113.38.11 address. Redistribution subject to ECS terms of use (see ecsdl.org/site/terms_use) unless CC License in place (see abstract).

Ga concentration effect

Figure 4 shows resistivity, Hall mobility and carrier concentration of bilayer GZO films for different Ga/(Zn+Ga) atomic ratios. Bilayer GZO films were prepared from GZO thin films, which were scanned 20 times and deposited on SiO_x buffer layers scanned 1 times by APPJ. The minimum resistivity of 6.00×10^{-4} Ω.cm was achieved at about 8 at% gallium doping. A possible explanation for this is that efficient occupation of Zn substitutional sites by Ga in the wurtzite structure (9), which resulted in the highest carrier concentration, 7.641×10^{20} cm^{-3}. The minimum mobility of 13.6 was achieved at approximately 8 at% gallium doping due to impurity scattering. Electrical properties of bilayer GZO films for different Ga concentration are summarized in Table I. The plots of $(\alpha h\nu)^2$ versus photon energy of bilayer GZO films deposited for different Ga/(Zn+Ga) atomic ratios, as shown in Fig. 5. Table II shows optical bandgap of bilayer GZO films for Ga doping concentration from 6 at% to 10 at%. According to Burnstein-Moss effect, the optical bandgap increased with an increase in carrier concentration. The maximum optical bandgap of 3.82 eV was achieved at approximately 8 at% gallium doping. The result is consistent with carrier concentration measured by Hall measurement, as shown in Table I. It is interesting to note that a decrease of optical bandgap is observed at 10 at%.

Table I. Electrical properties of bilayer GZO films scanned 20 times for different Ga concentration.

Gallium concentration	6 at%	8 at%	10 at%
Thickness (nm)	793	780	770
Sheet resistance (Ω/□)	8.9	7.7	10.0
Resistivity (Ω.cm)	7.09×10^{-4}	6.00×10^{-4}	7.70×10^{-4}
Hall mobility ($cm^2V^{-1}s^{-1}$)	18.0	13.6	14.1
Carrier concentration ($/cm^3$)	4.91×10^{20}	7.64×10^{20}	5.73×10^{20}

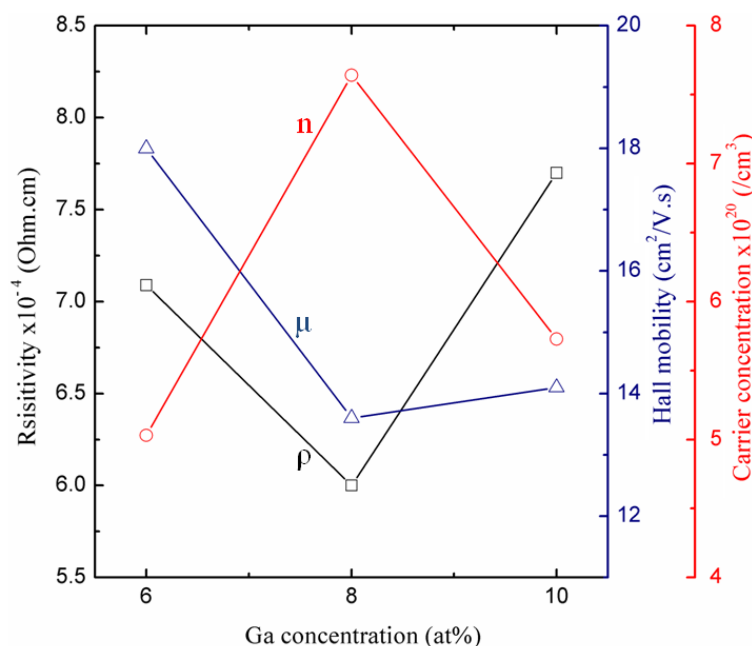

Figure 4. Resistivity (ρ), Hall mobility (μ) and carrier concentration (n) of bilayer GZO films deposited for different Ga/(Zn+Ga) atomic ratios.

Downloaded on 2014-04-28 to IP 140.113.38.11 address. Redistribution subject to ECS terms of use (see ecsdl.org/site/terms_use) unless CC License in place (see abstract).

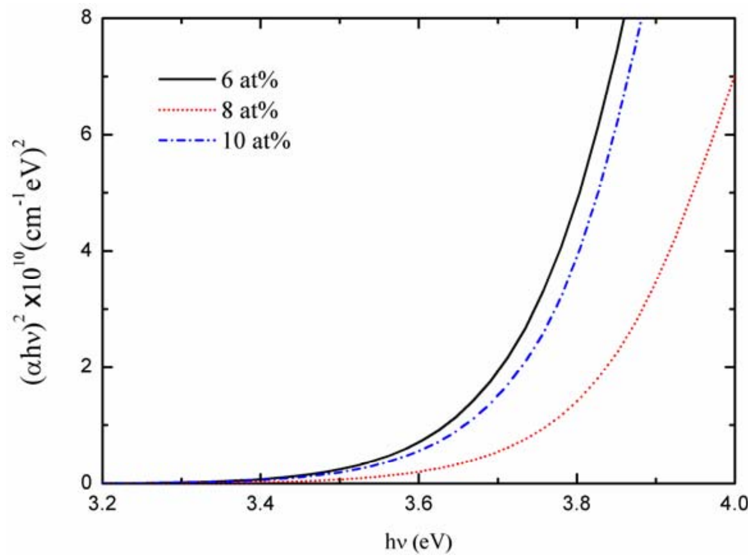

Figure 5. The plots of $(\alpha h\nu)^2$ versus photon energy of bilayer GZO films deposited for different Ga/(Zn+Ga) atomic ratios.

Table II. Optical bandgap of bilayer GZO films scanned 20 times for different Ga doping concentration.

Gallium concentration	6 at%	8 at%	10 at%
Optical bandgap (eV)	3.71	3.82	3.74

Scanning times effect

Figure 6 shows cross-sectional and surface SEM images of bilayer GZO films, which were scanned 10, 15 and 20 times by APPJ. SiO_x buffer layers deposited at argon carrier gas flow rates of 30 sccm and were scanned 1 times by APPJ. Thicknesses of bilayer GZO films measured by SEM were 450, 630 and 780nm for 10, 15 and 20 times, respectively. Owing to different flow rates between main gas and carrier gas, vortex was formed inside tube, which caused radicals have a long resident time, and resulted in formation of particles (10). As number of scans increase, bilayer GZO films shows thicker films, rougher surface morphologies and larger grain size. Figure 7 dipics absorption coefficient spectra of bilayer GZO for different scanning times, 10, 15 and 20times. In the ultraviolet region, the absorption coefficients decrease with an increase of Ga doping concentration (11). It can be speculated increasing scanning times could increase Ga/(Zn+Ga) atomic ratios. Figure 8 displays GIXRD patterns of bilayer GZO for different scanning times, 10, 15 and 20times. All bilayer GZO films exhibit preferred orientation along (002) plane. An increase in scanning times led to an increase in intensity of (002) peaks, as can be confirmed from Fig. 8. This results indicate a significant increase in crystallinity of bilayer GZO films. It worth noting that the ionic radius of Ga is smaller than Zn. Gallium incorporation caused lower lattice constant (12). There was a positive correlation between the lattice constant and d spacing. The Bragg angle was determined from d spacing. The positive shift in 2theta values of (002) peaks for bilayer GZO films resulted from increment of Ga doping concentration.

Downloaded on 2014-04-28 to IP 140.113.38.11 address. Redistribution subject to ECS terms of use (see ecsdl.org/site/terms_use) unless CC License in place (see abstract).

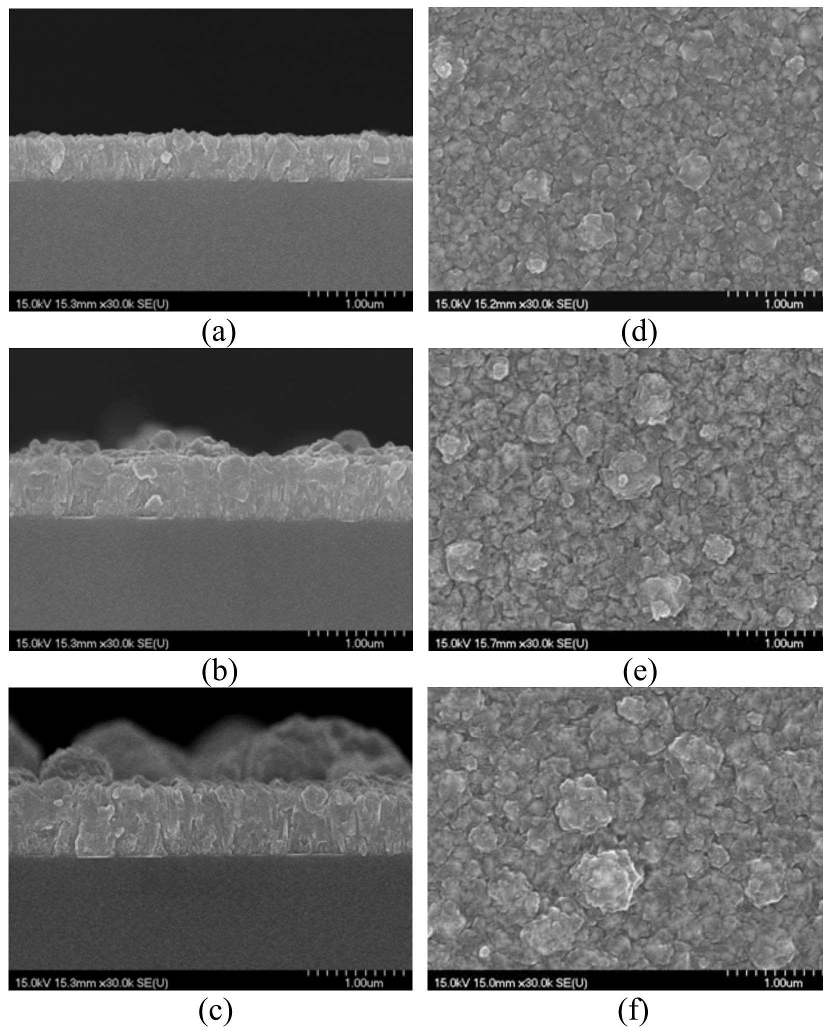

Figure 6. Cross-sectional and surface SEM images of bilayer GZO film scanned (a,d)10 times (b,e)15 times (c,f)20 times by APPJ. SiO_x buffer layers deposited at argon carrier gas flow rates of 30 sccm and were scanned 1 times by APPJ.

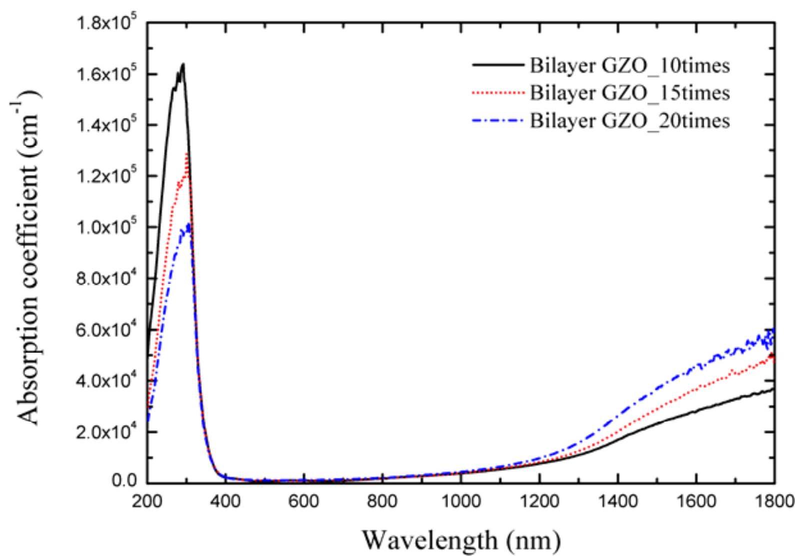

Figure 7. Absorption coefficient spectra of bilayer GZO for different scanning times: (a)10times (b)15times (c)20times.

Downloaded on 2014-04-28 to IP 140.113.38.11 address. Redistribution subject to ECS terms of use (see ecsdl.org/site/terms_use) unless CC License in place (see abstract).

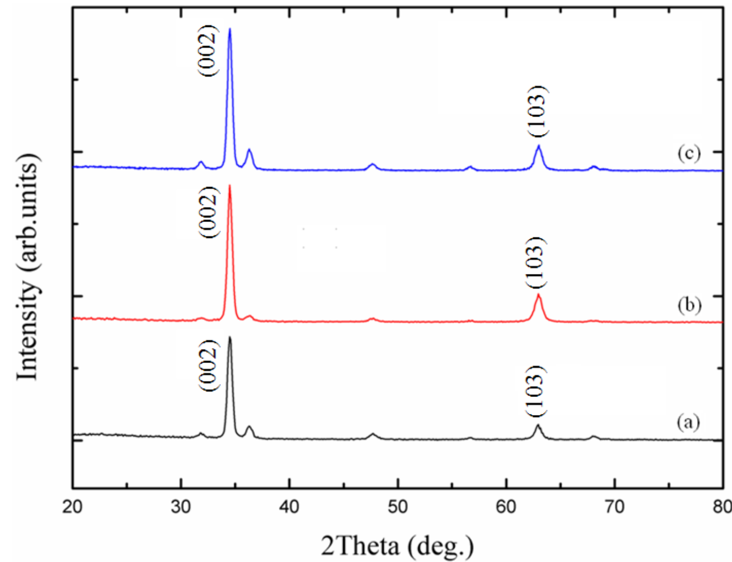

Figure 8. GIXRD patterns of bilayer GZO for different scanning times: (a)10times (b)15times (c)20times.

Table III compares electrical properties of Asahi U-type FTO and bilayer GZO films. The data do not show a significant increase in Hall mobility of bilayer GZO films. The resistivity of bilayer GZO film scanned 20 times was lower than Asahi U-type FTO film. This is attributed to high carrier concentration of bilayer GZO film deposited by scanning 20 times. Figure 9 shows the transmittance and haze of Asahi U-type FTO and bilayer GZO films of different number of scans, 10, 15 and 20 times. The transmittance in the 750-1100 nm region was lower than 80% for all bilayer GZO films due to high carrier concentration increasing free carrier absorption is shown in Fig. 9a. The bilayer GZO film scanned 20 times has much higher haze value in the visible and NIR regions, when compared to Asahi U-type FTO film and other bilayer GZO films, as shown in Fig. 9b.

Table III. Electrical properties of Asahi U-type FTO and bilayer GZO films.

	Asahi U-type FTO	Bilayer GZO		
Number of scans		10 times	15 times	20 times
Thickness (nm)	900	450	630	780
RMS (nm)	33.10	27.00	32.70	40.73
Sheet resistance (Ω/□)	8.2	19	11	7.7
Resistivity (Ω.cm)	7.38×10^{-4}	8.55×10^{-4}	6.93×10^{-4}	6.00×10^{-4}
Hall mobility ($cm^2V^{-1}s^{-1}$)	46.2	13.1	13.2	13.6
Carrier concentration ($/cm^3$)	1.830×10^{20}	5.573×10^{20}	6.823×10^{20}	7.641×10^{20}

Table IV. Optical (at 500nm) properties of Asahi U-type FTO and bilayer GZO films.

	Asahi U-type FTO	Bilayer GZO		
Number of scans		10 times	15 times	20 times
Transmittance (%)	83.0	84.0	83.2	81.0
Haze (%)	13.5	9.4	15.4	21.5

Downloaded on 2014-04-28 to IP 140.113.38.11 address. Redistribution subject to ECS terms of use (see ecsdl.org/site/terms_use) unless CC License in place (see abstract).

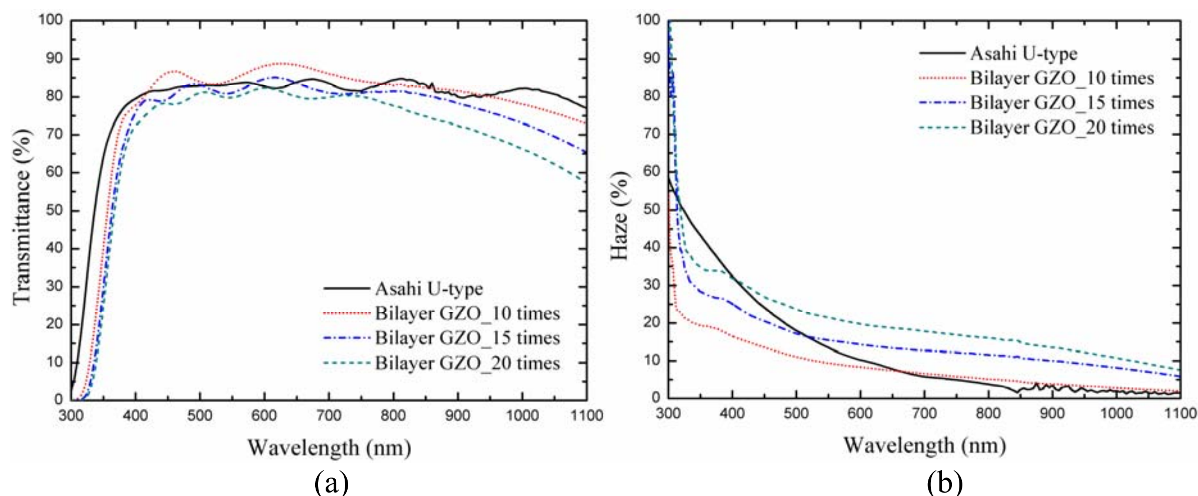

(a) (b)

Figure 9. (a)Transmittance (b)haze of Asahi U-type FTO film and bilayer GZO films of different number of scans, 10, 15 and 20 times.

Conclusion

In summary, the bilayer GZO film of high haze and low sheet resistance is achieved by APPJ. Thicknesses and RMS roughness of SiO_x buffer layers increase as argon carrier gas flow rates increase. With the increase in roughness of SiO_x buffer layer, bilayer GZO films have a significant increase in haze values. The minimum resistivity of 6.00×10^{-4} was achieved at 8 at% gallium doping, which has the highest carrier concentration. An increase in scanning times of deposition led to an increase in intensity of (002) main peaks, Hall mobility and carrier concentration. Thickness of bilayer GZO film was thinner than Asahi-U type FTO film and this result indicated that low material comsumption can be achieved by the APPJ deposition technique. The bilayer GZO film scanned 20 times has much higher haze value in the visible and NIR regions, when compared to Asahi U-type FTO film.

Acknowledgments

The authors are grateful for the support of this research by the Mechanical and Systems Research Laboratories, Industrial Technology Research Institute (ITRI).

References

1. Chia-Hua Huang, Hung-Lung Cheng, Wei-En Chang, Ming-Show Wong, *J. electrochem. Soc.*, **158**, H510 (2011).
2. Baosheng Sang, Katsumi Kushiya, Daisuke Okumura, Osamu Yamase, *Sol. Energy Mater. Sol. Cells*, **67**, 237 (2001).
3. E. Fortunato, L.Raniero, L.Silva, A.Gonc-alves, A.Pimentel, P.Barquinha, H.A´guas, L.Pereira, G. Goncalves, I.Ferreira, E.Elangovan, R.Martins, *Sol. Energy Mater. Sol. Cells*, **92**, 1605 (2008).
4. Joachim Muller, Bernd Rech, Jiri Springer, Milan Vanecek, *Sol. energy*, **77**, 917 (2004).
5. Mika Kambe, Makoto Fukawa, Naoki Taneda, Yukio Yoshikawa, Kazuo Sato, Kazuki Ohki, Shuichi Hiza, Akira Yamada, Makoto Konagai, *in Proceedings of 3rd World Conference on Photovoltaic Energy Conversion*, Osaka, Japan, IEEE (2003).

Downloaded on 2014-04-28 to IP 140.113.38.11 address. Redistribution subject to ECS terms of use (see ecsdl.org/site/terms_use) unless CC License in place (see abstract).

6. O. Kluth, B. Rech, L. Houben, S. Wieder, G. Schope, C. Beneking, H. Wagner, A. Loffl, H.W. Schock, *Thin solid films,* **351**, 247 (1999).
7. J. Krc, M. Zeman, O. Kluth, F. Smole, M. Topic, *Thin solid films,* **426**, 296 (2003).
8. K.M. Chang, S.H. Huang, Chin-Jyi Wu, Wei-Li Lin, Wei-Chiang Chen, Chia-Wei Chi, Je-Wei Lin, Chia-Chiang Chang, *Thin solid films,* **519**, 5114 (2011).
9. Dong-Won Kang, Seung-Hee Kuk, Kwang-Sun Ji, Seh-Won Ahn, Min-Koo Han, *Jpn. J. Appl. Phys.,* **49**, 031101 (2010).
10. Shih-Hsien Yang, Chi-Hung Liu, Chun-Hsien Su, Hui Chen, *Thin solid films,* **517**, 5284 (2009).
11. Mujdat Caglar, Saliha Ilican, Yasemin Caglar, Fahrettin Yakuphanoglu, *J. Mater. Sci.- Mater. Electron*, **19**, 704 (2008)
12. K.T. Ramakrishna Reddy, H. Gopalaswamy, P.J. Reddy, R.W. Miles, *J. Cryst. Growth*, **210**, 516 (2000)

Downloaded on 2014-04-28 to IP 140.113.38.11 address. Redistribution subject to ECS terms of use (see ecsdl.org/site/terms_use) unless CC License in place (see abstract).